ESI

1. High-Pressure Crystallisation of Biodiesel

High-pressure studies using Raman spectroscopy and optical imaging in this work suggested that biodiesel crystallises under high pressure. However, no diffraction studies of biodiesel or relevant main components under high pressure have been reported in the literature.

Raman spectra were recorded at ambient temperature (*ca.* 293 K) on a sample of biodiesel contained within a Merrill-Bassett diamond-anvil cell (DAC),[14] equipped with 600 μm culets and a tungsten gasket with a 250 μm hole. A small number of ruby spheres were also loaded as the pressure calibrants. The ruby fluorescence method was used to determine the pressure.[15–17] Raman spectra were recorded on a Jobin-Yvon LabRam 300 spectrometer equipped with a 50 mW He-Ne laser of wavelength 632.8 nm.

The main components of biodiesel are long-chain methyl esters, with varying chain length, degree of saturation, and distribution of double bonds.[1] These hydrocarbon groups mainly include medium-chain (C10 – C14), long-chain (C16 – C18), very-long-chain (≥ C20), and fatty acid derivatives. However, Raman spectroscopy is insensitive to the fatty acids with chain-length > 11.[2,3] The presence of unsaturated carbon-carbon double bonds gives rise to specific vibration bands, while the individual location of carbon double bonds do not induce differences in the spectrum.[4] However, conjugated double bonds in the methylene chain lead to a high intensity fluorescence background, which can overwhelm the characteristic vibrational bands of a sample. The feedstock for the biodiesel used in this work is soybean oil, and hence the fatty acid methyl stearates can be expected to be predominantly unsaturated and give rise to a large fluorescent background.[5] Indeed, this background was observed in the experimental Raman spectra of biodiesel (**Figure S1**). With increasing pressure, the intensity of the fluorescence background becomes weaker. Combining with the results from high-pressure X-ray powder diffraction studies (**Figure S4**), it may suggest that at high pressure conditions, biodiesel partially forms typical mesomorphous ordered structures.[6,7] Due to the amphiphilic conformation of fatty acid methyl esters, it most likely to form smectic type crystals. This type of crystal exhibits ordering through layers perpendicular molecular axis, and remains ordered in the remaining two dimensions. Alternatively, it is possible that the amphipilic molecules may form lamellar micelles upon compression. Formation of such structures is also known to reduce fluorescence intensity.[7–9]

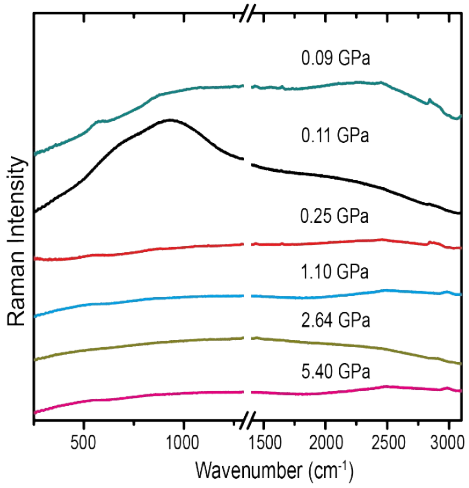

Figure S1. Raman spectra of Biodiesel at selected pressures under room temperature. Characteristic peaks of diamond anvils were chopped off from spectra.

High-pressure X-ray powder diffraction measurements were conducted at ambient temperature on biodiesel sample compressed in a Merrill-Bassett DAC, equipped with 600 μm culets and a tungsten gasket with a 250 μm hole. A few of ruby spheres were also loaded in as the pressure calibrants. The pressure was increased directly from ambient pressure to 1.3 GPa. Needle-shaped crystals were formed during this process. A hot air gun was employed to melt these crystals, and then the sample was placed immediately in the freezer (about -20 °C) to form polycrystalline material. The pressure was increased from 1.3 GPa to 3.2 GPa stepwise. **Figure S2** shows the 2D X-ray powder diffraction patterns that were recorded at room temperature on the Extreme Conditions Beamline (I15), at the Diamond Light Source. (λ = 0.413400 Å). Samples were exposed in the X-ray beam for 120 s. 2D diffraction patterns were recorded by a Mar345 image-plate detector. Images were processed to give powder-diffraction patterns of intensity against diffraction angle 2θ using the software Fit2D.

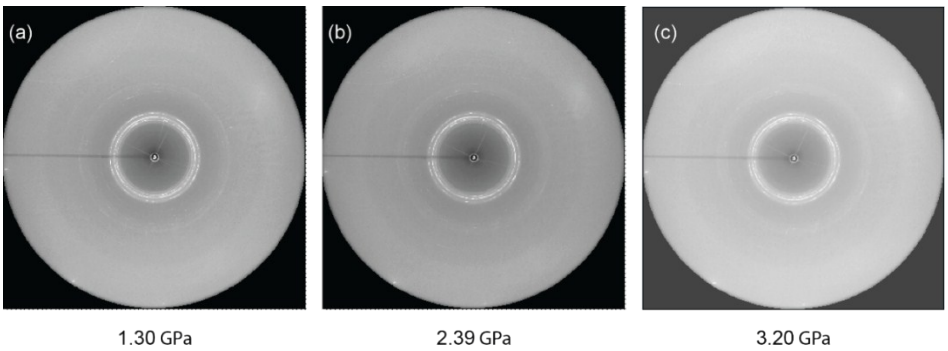

Figure S2. 2D X-ray powder diffraction images of biodiesel at selected pressures in the compression process. Data were collected at I15, Diamond Light Source (λ = 0.4134 Å). (**a**) biodiesel at 1.30 GPa, (**b**) biodiesel at 2.39 GPa, and (**c**) biodiesel at 3.20 GPa.

Rather than one single crystal, powder samples contain many crystallites oriented at random. This would induce concentric cones of diffracted intensity emanating from the sample, shown as a series of concentric rings on the detector. The 2D powder diffraction images of biodiesel collected during the compression process suggested high quality powder patterns with some degree of preferred orientations shown as broken rings.

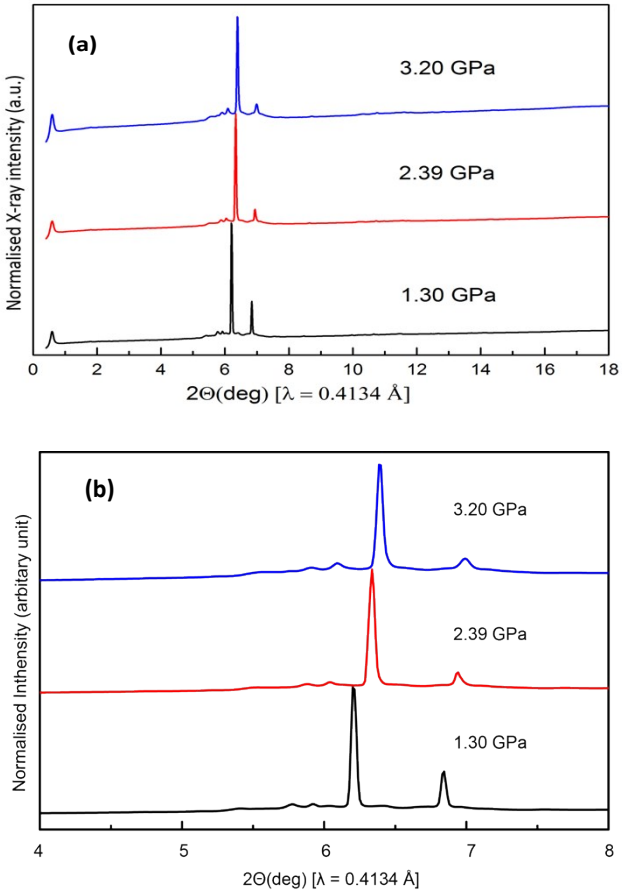

Figure S3. X-ray powder diffraction patterns of biodiesel obtained when the pressure increased from 1.3 GPa to 3.2 GPa. (**a**) multiplot the full range of XRPD patterns of biodiesel; (**b**) zoom-in to highlight the similarities shown in the compression process.

The 2D diffraction images were converted into diffraction patterns by Fit2D, shown in **Figure S3**. All XRPD patterns of biodiesel are remarkably similar to each other. The shifts along the x-axis were caused by compression of the lattice, leading to a decrease in *d*-spacing. The significant similarity shown in the XRPD patterns suggests that the biodiesel sample did not change when the pressure increased over this pressure range.

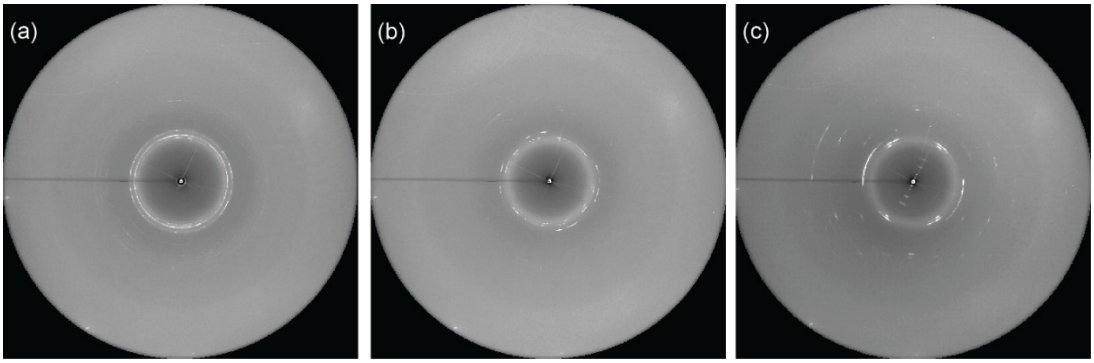

Figure S4. Raw X-ray powder diffraction images of biodiesel at selected pressures in the decompression process. Data were collected at I15, Diamond Light Source ($\lambda = 0.4134$ Å). (**a**) biodiesel at 1.07 GPa, (**b**) biodiesel at 0.36 GPa, and (c) biodiesel at 0.16 GPa.

The pressure was then decreased from 3.20 GPa to 0.16 GPa. The XRPD patterns are shown in **Figure S3**. All the patterns of biodiesel are similar to each other. However, there are still some variations between each pattern, both in terms of relative intensities and some peak positions. More precisely, there is a strong low-angle peak ($2\theta = 0.8°$) in the patterns of biodiesel at 3.20 GPa and 1.07 GPa. However, this strong peak changed into a weak one when the pressure decreased to 0.36 GPa. In the meantime, in the patterns of biodiesel at 3.2 GPa and 1.07 GPa, there was one strong peak followed by a weak one in the range of $2\theta = 6° - 8°$. When the pressure decreased to 0.36 GPa, these peaks changed into two strong peaks. This suggests that there is a possible phase transition of biodiesel when the pressure decreased from 1.07 GPa to 0.36 GPa. When sample was decompressed to 0.16 GPa, the relative intensities of these two strong peaks changed again. This suggests that there is another possible phase transition of biodiesel when the pressure over this pressure range. However, as it shown in **Figure S4**, the smeared diffracted intensities along the Debye-Scherrer rings suggest that the quality of the polycrystallied powder sample of biodiesel was very poor. In the meantime, it shows clearly in these 2D images that when the pressure decreased, the preferred orientation became greater. The conclusions about phase transitions based on XRPD data are therefore not promising.

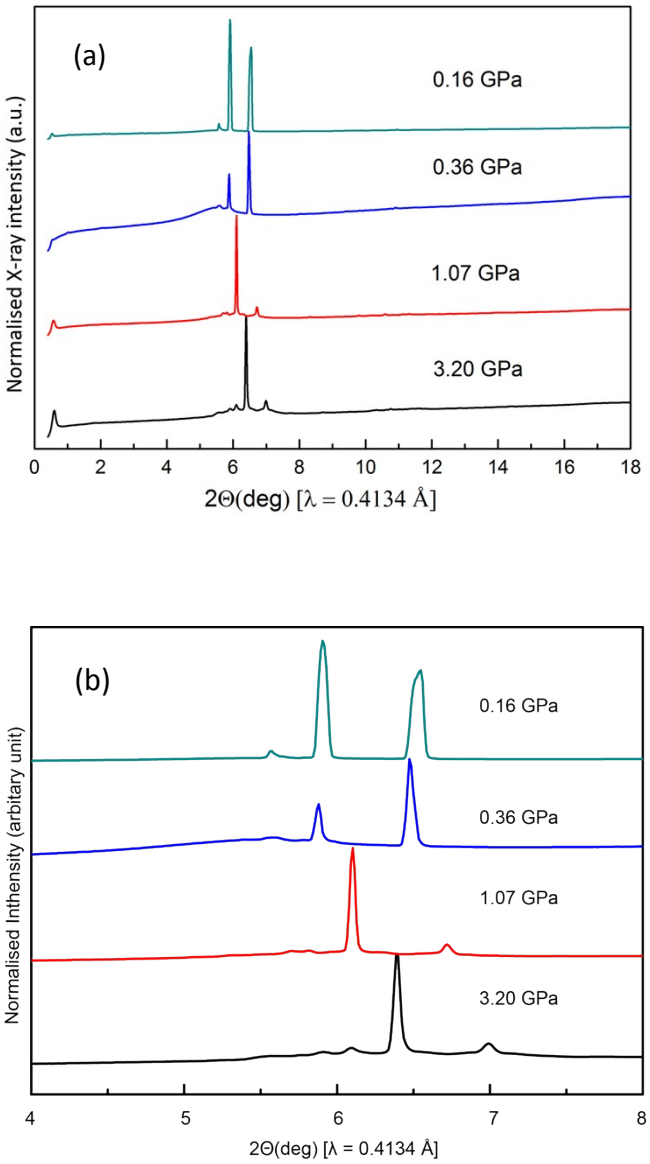

Figure S5. XRPD patterns of biodiesel obtained in the decompression process. (**a**) multiplot the full range of XRPD patterns of biodiesel; (**b**) zoom-in to highlight the differences shown in the decompression process.

The XRPD pattern of biodiesel is formed by the patterns convolution of a large number of FAMEs and relevant derivatives. The strong amorphous background, shown in each patterns of biodiesel in **Figure S3** and **Figure S5**, suggests that biodiesel partially crystallised in both the compression pressure range of 1.30 GPa to 3.20 GPa, and the decompression pressure range of 3.2 GPa to 0.16 GPa. The lack of knowledge of the chemical compositions of biodiesel crystals induced by pressure, coupled with the poor quality of XRPD from the poor quality of crystal due to nature of flexibility of long-chain molecules, meant that structure solution of biodiesel crystals induced by high pressure is impossible.

2. High-Pressure Crystallisation of Methyl Stearate

Table S1. Unit cell parameters of Form III at selected pressures

p(GPa)	*a* (Å)	*b* (Å)	*c* (Å)	*β* (°)	*V* (Å³)	R_{wp} (%)
0.11	95.758(1)	7.326(1)	5.586(7)	92.55(8)	3915(5)	1.836
0.18	95.316(1)	7.237(3)	5.537(9)	93.10(6)	3814(6)	2.127
0.36	95.211(9)	7.178(6)	5.503(1)	93.35(9)	3754(10)	2.278
0.44	95.097(7)	7.168(4)	5.490(2)	93.38(1)	3736(7)	2.164
0.48	95.011(8)	7.143(6)	5.468(5)	93.50(1)	3704(7)	2.067
0.63	94.877(9)	7.095(3)	5.433(7)	93.67(2)	3650(9)	1.998
0.87	94.775(9)	7.060(7)	5.408(9)	93.81(7)	3611(3)	1.950
1.05	94.558(7)	7.021(1)	5.380(4)	93.97(3)	3563(1)	2.138
1.22	94.381(1)	6.978(1)	5.350(8)	94.13(5)	3514(9)	1.874
1.50	94.052(9)	6.914(1)	5.307(8)	94.38(1)	3441(6)	2.018

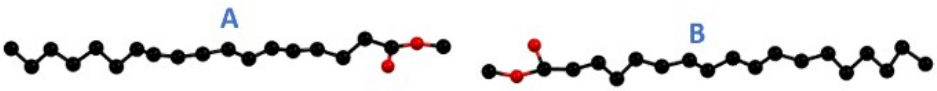

Figure S6. The asymmetric unit of the crystal structure of Form II of methyl stearate at 0.11 GPa. All hydrogen atoms are omitted for clarity. Atoms are coloured as C (black) and O (red).

Figure S6 shows the asymmetric unit of Form III at 0.11 GPa. After Rietveld refinement of atomic positions with bond angle- and length-restraints, the crystal structure still shows some degrees of disorder with respect to the conformation of hydrocarbon chain and ester groups in molecule B. However, due to the limited quality of HP-XRPD data, combined with the complexity of the crystallographic structure of MS, no further refinements could be performed on current stage.

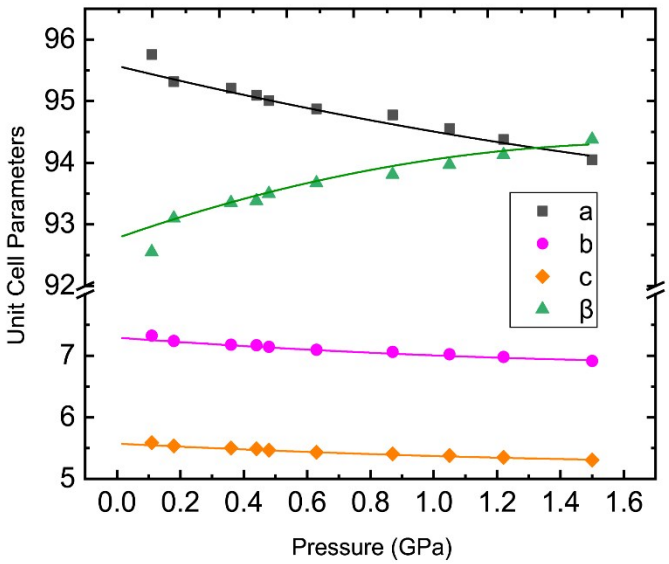

Figure S7. Compression of the unit cell parameters (a, b, c, and β) of Form III of methyl stearate in the pressure range of 0.11 GPa to 1.50 GPa, as determined by Rietveld refinements.

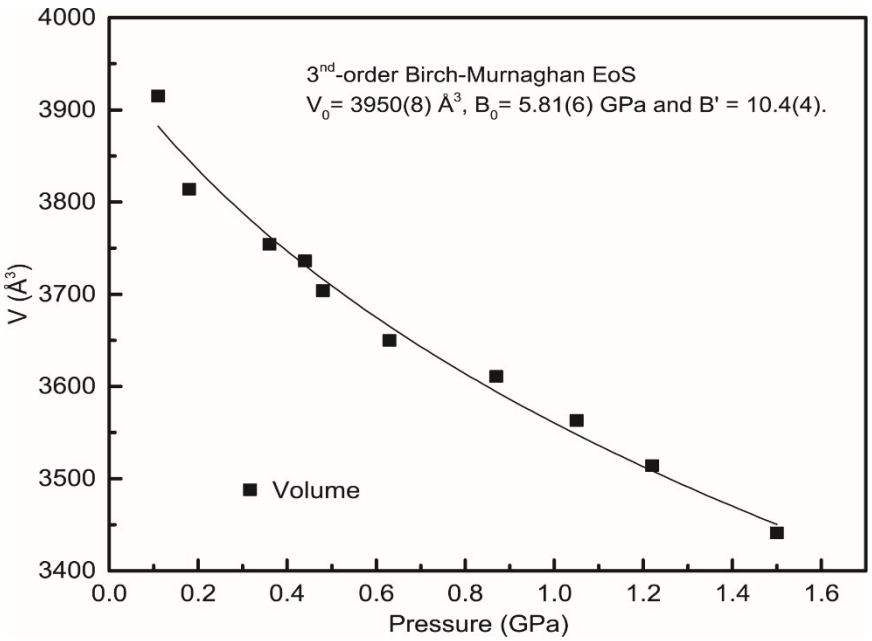

Figure S8. p-V plot for Form III of methyl stearate. The compression of the unit cell volume with pressure has been fitted to a 3rd-order Birch-Murnaghan EoS.

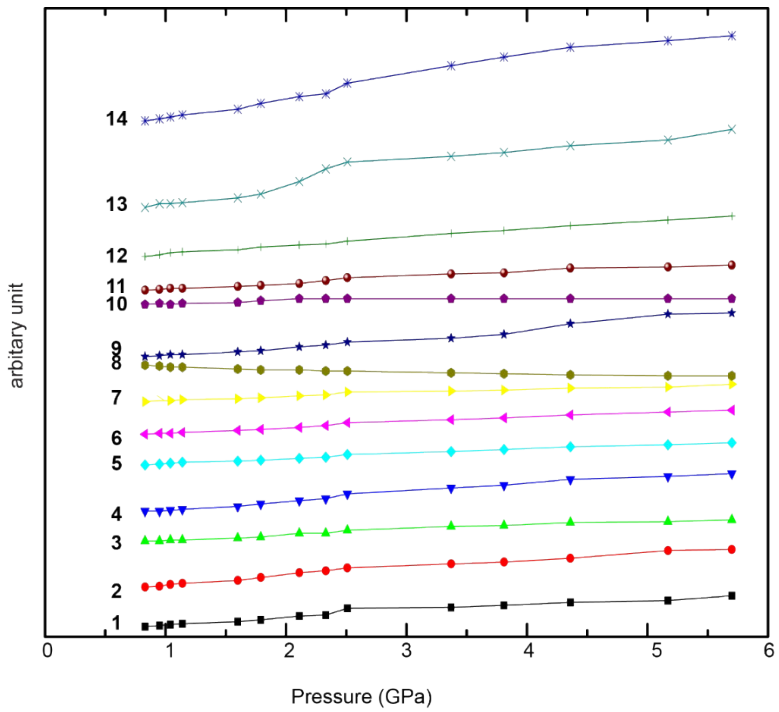

Figure S9. Multiplot of pressure dependence of the frequency of the characteristic vibration of methyl stearate at the compression process over the pressure range of 0.83 GPa to 5.70 GPa. Numbers of each plot lines correspond to the peaks labelled in **Figure 5**.

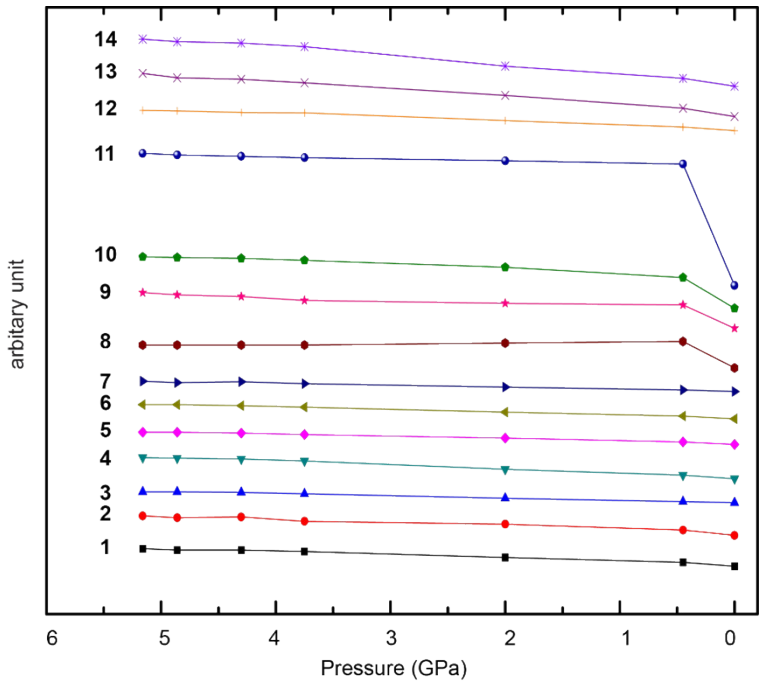

Figure S10. Multiplots of pressure dependence of the frequency of the characteristic vibration of methyl stearate on decompression. The pressure was reduced from 5.16 GPa to ambient pressure. Numbers of each plot lines correspond to the peaks labelled in **Figure 5**.

A polycrystalline sample of Form V of deuterated methyl stearate was loaded into the PE cell with a lead chip as the pressure marker together with a few drops of Fluorinert (FC-87) as the pressure-transmitting medium. A pressure of 0.57 GPa was initially applied in order to seal the cell. A 2 hour data collection was conducted using the $2\theta = 90°$ detectors at room temperature over the *d*-spacing range of 1.0 Å to 4.2 Å. According to the high-pressure X-ray powder diffraction experiments, the phase transition of Form V to Form III occurs at pressures lower than 0.11 GPa. Rietveld refinements (**Figure S10**) were therefore performed on the neutron powder diffraction pattern using the GSAS program to identify the starting form for this high-pressure experiment. Both crystal structures of Form III at 0.11 GPa and Form V were used as model structures. Due to the complexity of the structure of methyl stearate, atomic coordinates and thermal parameters were not refined.

The complexity of the crystal structure of methyl stearate results in a very complex pattern indicated by pink tick marks in **Figure S10**. In addition to the Bragg peaks from methyl stearate sample, the pressure calibrant (Pb), and other impurities from the sample environment (ZrO_2 and Al_2O_3, respectively) all contribute to the experimental patterns collected on the PEARL beamline using the PE press. By close visual inspection of the final fit of the Rietveld refinements for the neutron powder pattern collected at 0.57 GPa, the calculated reflections from these 4 different materials can be matched with all the experimental reflections in both final fits of the Rietveld refinements based on both model structures. There were few mismatches of intensities shown in the Rietveld refinement performed with the structure of Form III of methyl stearate at 0.11 GPa. However, the thermal parameters and preferred orientation, which could potentially affect the relative intensities, were not refined in this experiment due to the complexity of the structure. The form of methyl stearate therefore could not be conclusively identified on the basis of the Rietveld refinements in this experiment, although on balance the pattern corresponds most closely to Form V rather than Form III.

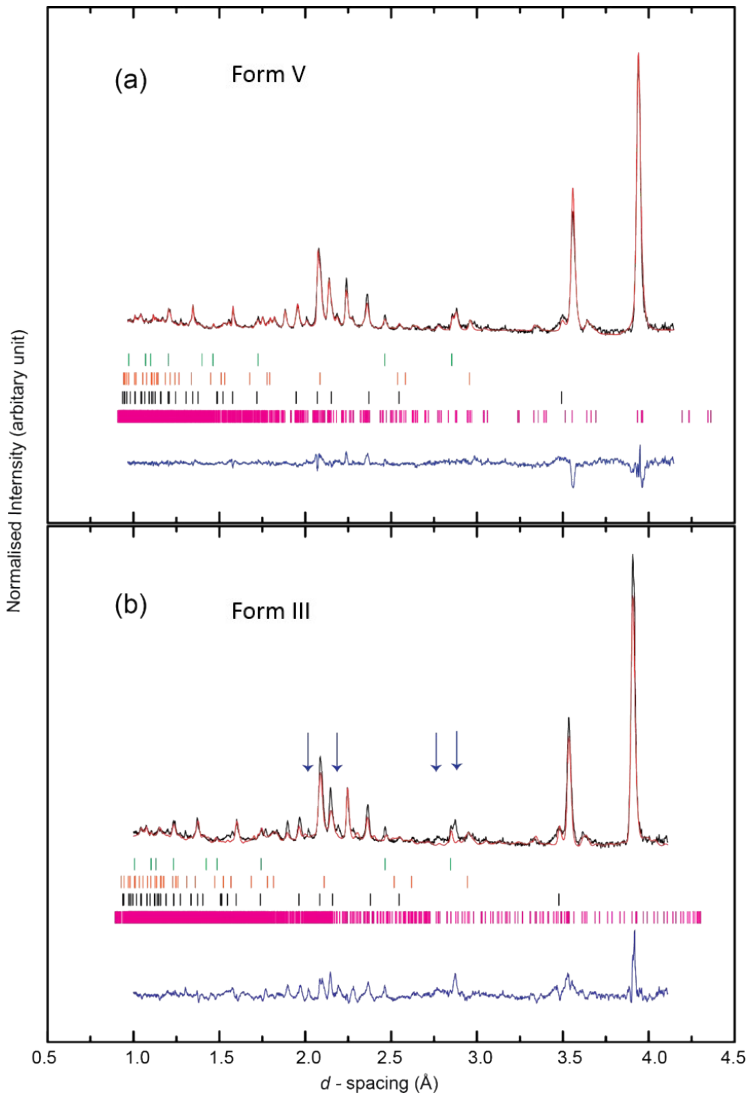

Figure S11. Best fits for the Rietveld refinement of the high-pressure neutron powder pattern of methyl stearate collected at 0.57 GPa / 298 K. Both crystal structures of Form III at 0.11 GPa (**b**) and Form V of methyl stearate (**a**) were employed as model structures. In both cases the experimental profile (—), calculated profile (—) and difference (—). Vertical tick values for each phase are shown for clarity: methyl stearate (pink), Al_2O_3 (black), ZrO_2 (orange) and Pb (green). Blue arrows indicate mis-matching reflections.

In order to confirm this, the sample was decompressed and loaded into a vanadium can (without the lead chips). Neutron powder diffraction data were recorded for 20 min using the 2θ = 90° detector at room temperature on the PEARL beamline. It was then plotted together with the neutron powder pattern (Bank 2) of Form V collected on the HRPD beamline; as well as the powder pattern simulated from the crystal structure of Form III of methyl stearate at 0.11 GPa based on the PEARL instrument parameter file (**Figure S12**). The comparison of the patterns shows clearly that the powder pattern collected in the vanadium can at ambient condition (**Figure S12b**) is similar as that of Form V of methyl stearate collected on the HRPD facility at 193 K. The differences reflect the higher resolution of the HRPD instrument and the shift of peaks due to the temperature differences. The simulated powder pattern of the Form III at 0.11 GPa (**Figure S12a**) is significantly different from others, especially in the *d*-spacing

range of 1.5 Å to 2.5, whilst the strong peak, shown at *ca. d*-spacing = 2.9 Å in **Figure S12b** and **Figure S12c**, is not observed in this pattern.

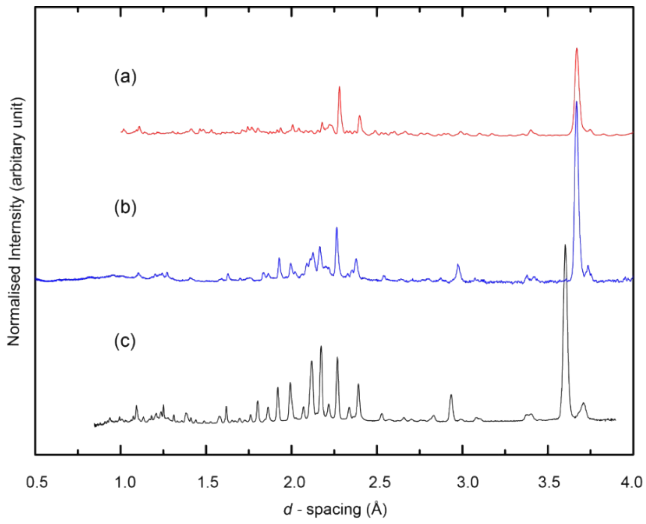

Figure S12. Comparison of neutron powder patterns of methyl stearate: (**a**) simulated pattern Form III of methyl stearate at 0.11 GPa using the PEARL instrumental file, (**b**) powder pattern of methyl stearate in vanadium can collected on the PEARL instrument at ambient condition, (**c**) powder pattern of Form V of methyl stearate recorded at 193 K (Bank 2) on the HRPD facility.

Table S2. Unit cell parameters of Form V of deuterated methyl stearate at selected pressures

p (GPa)	*a* (Å)	*b* (Å)	*c* (Å)	*β* (°)	*V* (Å^3)	R_{wp} (%)
0.57	48.519(5)	7.061(4)	5.425(13)	76.54(13)	1807.85(1)	0.064
0.58	48.517(8)	7.057(1)	5.424(8)	76.52(6)	1806.32(3)	0.114
1.04	48.295(1)	6.931(7)	5.352(6)	75.99(12)	1738.41(1)	0.073
1.28	48.200(3)	6.876(9)	5.319(4)	75.70(9)	1708.41(9)	0.073
1.39	48.177(4)	6.863(9)	5.312(3)	75.63(13)	1701.61(9)	0.068
1.43	48.172(5)	6.859(2)	5.309(8)	75.61(6)	1699.44(5)	0.073
1.50	48.143(9)	6.842(9)	5.298(13)	75.53(1)	1690.17(6)	0.072
1.58	48.116(10)	6.828(3)	5.290(5)	75.46(7)	1682.70(9)	0.070
1.63	48.089(3)	6.815(1)	5.281(7)	75.39(10)	1674.99(1)	0.075
1.71	48.071(5)	6.800(3)	5.273(9)	75.33(4)	1667.80(9)	0.070
1.79	48.053(4)	6.789(6)	5.266(3)	75.26(7)	1661.88(3)	0.093
1.95	47.999(4)	6.756(3)	5.245(2)	75.10(1)	1644.10(4)	0.086
2.17	47.954(1)	6.727(5)	5.224(2)	74.94(5)	1627.46(3)	0.090
2.59	47.843(10)	6.669(7)	5.188(7)	74.63(4)	1596.38(5)	0.092
2.83	47.789(6)	6.640(3)	5.173(1)	74.48(10)	1581.90(5)	0.084
2.91	47.781(10)	6.629(8)	5.167(8)	74.43(2)	1576.72(2)	0.093
3.31	47.659(13)	6.581(3)	5.137(8)	74.15(7)	1550.39(9)	0.125

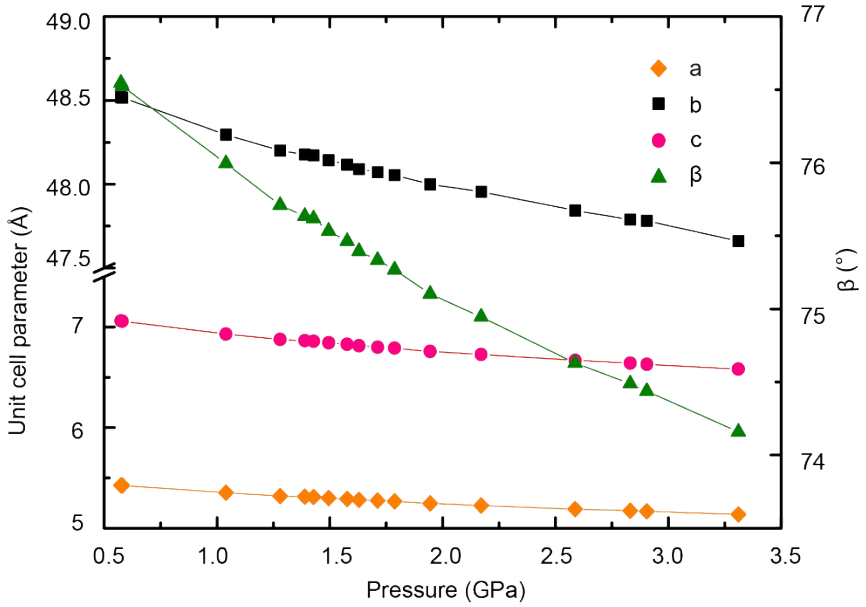

Figure S13. The compression behaviour of the unit-cell parameters of deuterated methyl stearate (Form V) in the pressure range of 0.57 GPa to 3.31 GPa, as determined by the Rietveld refinement.

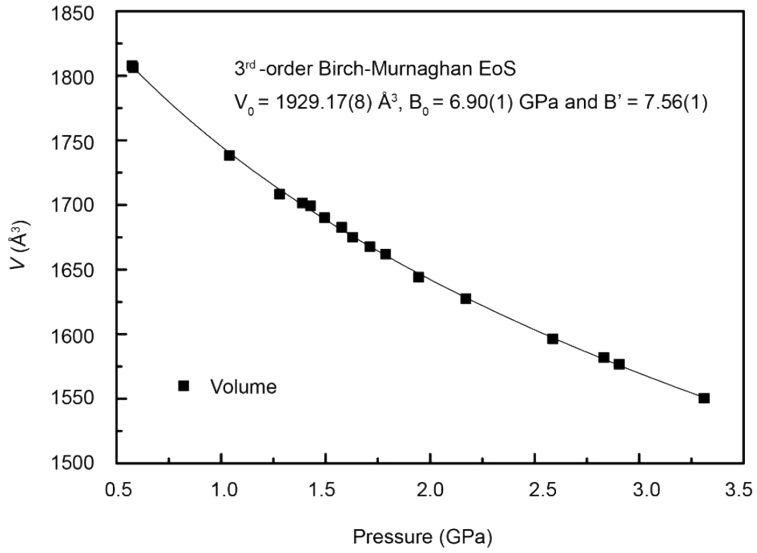

Figure S14. PV plot for Form V of deuterated methyl stearate. The compression of the unit cell volume with pressure has been fitted to a 3rd-order Birch-Murnaghan EoS.

To confirm the identity of the initial phase at the first pressure point (0.57 GPa), a sample was unloaded from the PE press and loaded into a vanadium can without Pb chips. Neutron powder diffraction data were recorded for 20 min using the 2θ = 90° detector at room temperature on the PEARL beamline. Rietveld refinements (**Figure S15**) were performed using the crystal structure of Form V of deuterated methyl stearate as the structural model. The reasonable fit of the Rietveld refinement (R_{wp} = 6.0 % and R_p = 5.44 %) confirmed that the sample recovered from 0.57 GPa in the high-pressure neutron experiment was indeed Form V.

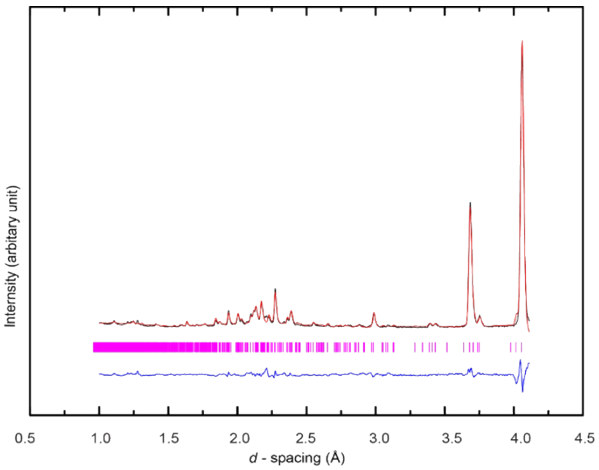

Figure S15. Rietveld plot of neutron powder data of deuterated methyl stearate collected at ambient conditions in vanadium can on the PEARL beamline. The experimental profile (—), calculated profile (—) and difference (—). Vertical tick values (I) show calculated peak positions. The good fit indicates the sample was form V.

References:

1 S. Bresson, M. El Marssi and B. Khelifa, *Chem. Phys. Lipids*, 2005, **134**, 119–29.

2 Y. Y. Huang, C. M. Beal, W. W. Cai, R. S. Ruoff and E. M. Terentjev, *Biotechnol. Bioeng.*, 2010, **105**, 889–898.

3 Q. Hu, M. Sommerfeld, E. Jarvis, M. Ghirardi, M. Posewitz, M. Seibert and A. Darzins, *Plant J.*, 2008, **54**, 621–639.

4 A. M. Miranda, E. W. Castilho-Almeida, E. H. Martins Ferreira, G. F. Moreira, C. A. Achete, R. A. S. Z. Armond, H. F. Dos Santos and A. Jorio, *Fuel*, 2014, **115**, 118–125.

5 M. F. Milazzo, F. Spina, S. Cavallaro and J. C. J. Bart, *Renew. Sustain. Energy Rev.*, 2013, **27**, 806–852.

6 T. Moriya, O. Nakanishi, A. Yanase and M. Kataoka, *Springer Series in Solid-State Sciences*, 1981, vol. 29.

7 Z. Y. Cheng, B. Y. Ren, S. Y. He, X. X. Liu and Z. Tong, *Chinese Chem. Lett.*, 2011, **22**, 1375–1378.

8 V. Cherezov, J. Liu, M. Griffith, M. A. Hanson and R. C. Stevens, *Cryst. Growth Des.*, 2008, **8**, 4307–4315.

9 V. Cherezov, J. Clogston, M. Z. Papiz and M. Caffrey, *J. Mol. Biol.*, 2006, **357**, 1605–1618.

10 M. M. Batenjany, T. J. O'Leary, I. W. Levin, J. T. Mason, T. J. O. Leary, W. Ira and J. T. Mason, *Biophys. J.*, 1997, **72**, 1695–1700.

11 J. R. Beattie, S. E. J. Bell and B. W. Moss, *Lipids*, 2004, **39**, 407–419.

12 G. Socrates, *Infrared and Raman characteristic group frequencies*, 2004.

13 R. Silverstein, F. Webster, D. Kiemle and D. Bryce, *Spectrometric Identification of Organic Compounds*, 2014.

14 G. D. Saraiva, J. R. Maia, J. A. Lima, C. E. S. Nogueira, P. T. C. Freire, F. F. de Sousa, A. M. R. Teixeira and J. Mendes Filho, *Spectrochim. Acta - Part A Mol. Biomol. Spectrosc.*, 2017, **184**, 327–334.

15 E. N. Lewis, R. Bittman and I. W. Levin, *BBA - Biomembr.*, 1986, **861**, 44–52.